AMERICAN SOCIETY of
GENE & CELL
THERAPY

PD-1 IC Inhibition Synergistically Improves Influenza A Virus-Mediated Oncolysis of Metastatic Pulmonary Melanoma

Siarhei Sitnik,[1,2] Dörthe Masemann,[1,2] Rafael Leite Dantas,[1] Viktor Wixler,[1,3] and Stephan Ludwig[1,3]

[1]Institute of Molecular Virology (IMV), Centre for Molecular Biology of Inflammation (ZMBE), Westfaelische Wilhelms University, 48149 Muenster, Germany

Recently, we showed that infection of primary lung tumor-bearing mice with oncolytic influenza A viruses (IAVs) led to strong virus-induced tumor cell lysis but also to restoration of immune competence of innate immune cells. Murine B16-F10 melanoma cells are known for their high lung tropism and progressive growth. As these cells are also highly permissive for IAVs, we analyzed their oncolytic and immunomodulatory efficiency against pulmonary B16-F10 lung metastases *in vivo*. IAV infection abrogated the melanoma-mediated immune suppression in the lung and induced a more than 50% cancer cell lysis. The oncolytic effect reached maximal efficacy 3 days post-infection, but it was not sustained over time. In order to maintain the virus-induced anti-tumor effect, mice with melanoma-derived lung cancers were treated in addition to influenza virus infection with an immune checkpoint inhibitor against programmed death-1 receptor (PD-1). The combined IAV and immune checkpoint inhibition (ICI) therapy resulted in a sustained anti-tumor efficacy, keeping the lung melanoma mass at day 12 of IAV infection still reduced by 50% over the control mice. In conclusion, ICI treatment strongly enhanced the oncolytic effect of influenza virus infection, suggesting that combined treatment is a promising approach against metastatic pulmonary melanoma.

INTRODUCTION

Melanoma is the most aggressive and deadly type of skin cancer. It easily spreads throughout the body, primarily to the lung, and the 5 year-survival rate of patients with stage IV melanoma having lung metastases does not exceed 21%.[1] Successful treatment of lung metastases in general and melanoma lung metastases in particular is still a great challenge for tumor therapy. In addition, progressively growing melanoma tumors and their lung metastases develop a strong immunosuppressive tumor microenvironment (TME) based on overexpression of immune checkpoint (IC) molecules and secretion of anti-inflammatory mediators.[2,3] The current protocols with the best perspective for treatment of advanced melanomas therefore include targeted chemotherapy, application of oncolytic viruses (OVs), and IC inhibition (ICI), which seek to break down the TME and reprogram tumor-associated immune cells back toward a tumoricidal phenotype.

In the context of primary melanoma therapy, oncolytic virotherapy offers broad therapeutic perspectives. On the one hand, replication of OVs causes tumor cell lysis and remodeling of TME.[4] On the other hand, primary viral infection induces a massive release of tumor-associated antigens and induces expression and secretion of pro-inflammatory cytokines, which in turn promotes repolarization and additional recruitment of immune cells, thus introducing a secondary immune-mediated oncolysis. Talimogene laherparepvec (T-VEC) is the first therapeutically approved OV to treat unresectable primary melanoma, but many other OVs constructed on the background of adenoviruses, picornaviruses, and herpesviruses are now undergoing advanced clinical trials against melanoma.[5,6] Nevertheless, a significant number of patients respond poorly to the immunotherapy or do not respond at all (reviewed in Martinez-Quintanilla et al.[5] and Byrne et al.[7]). Furthermore, application of OVs can be applied only locally to target the primary cancer, thus being inefficient against metastatic pulmonary melanoma in patients.

In this respect, influenza A viruses (IAVs) are gaining strong scientific interest as OVs for treatment of pulmonary carcinomas, because lung cells are the primary targets for IAVs and are naturally permissive for IAV infection. Many primary lung carcinomas originate from type II pneumocytes, the neoplastic transformation of which is based on constitutive activation of the Raf/MEK (mitogen-activated protein kinase kinase)/ERK (extracellular signal-regulated kinase) signaling cascade. This cascade is also pivotal for replication of IAV.[8-10] In a pre-clinical immunocompetent murine model for non-small-cell lung carcinoma (NSCLC), we recently demonstrated a strong oncolytic efficacy of sublethal IAVs against this type of lung carcinoma complemented with restoration of immunocompetence of tumor-associated macrophages upon intranasal application.[6] The tumor-bearing mice tolerated IAV infection even better than did control mice, due to preferential infection and replication of IAV in NSCLC cells over normal lung tissue cells. Interestingly, other recently
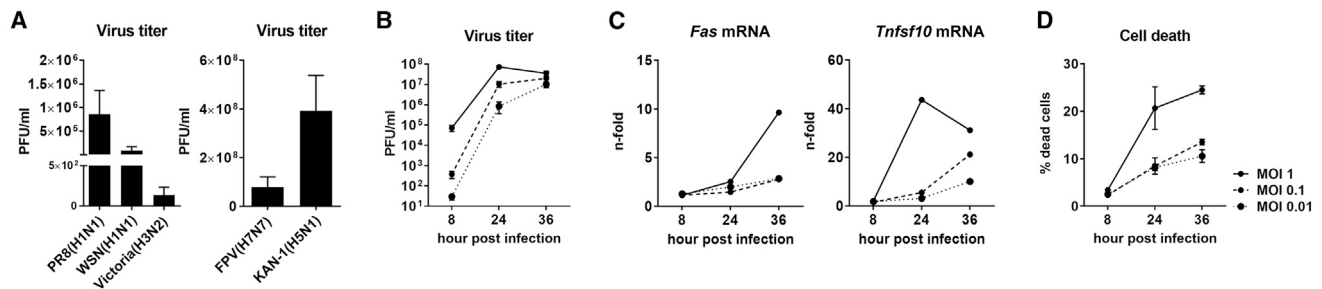
Figure 1. Murine B16-F10 Melanoma Cells Are Highly Permissive for IAV Infection

(A) B16-F10 cells were infected with different low pathogenic human (left panel) or highly pathogenic avian IAV strains (right panel) and virus titers in cell supernatants were determined by standard plaque assay at 24 h post-infection (hpi). B16-F10 cells were infected with an MOI of 0.01 with low pathogenic human IAVs (strains PR8, WSN, and Victoria) or a MOI of 0.001 with highly pathogenic avian IAVs (strains FPV and KAN-1). Virus titers are presented as plaque-forming units (PFU) per mL. (B) B16-F10 cells were infected with PR8 of different MOIs, and virus titers represented as PFU/mL were investigated at indicated time points post-infection by standard plaque assay. (C) mRNA expression levels of *Fas* and *Tnfsf10* as marker genes for apoptosis induction were evaluated by qRT-PCR at different times of IAV infection. (D) Induction of cell death upon PR8 infection was investigated by fixable viability dye eFluor 450 staining and subsequent flow cytometry analysis at different time points post-infection. Mean values of three independent experiments ± SEM are shown.

published studies demonstrated a permissivity of melanoma cell lines for IAV *in vitro* and an oncolytic effect of IAVs against non-metastasizing progressively growing melanoma *in vivo*.[11,12]

Besides OVs, several checkpoint inhibitors have been developed and successfully approved as immunomodulatory anti-cancer agents. The most prominent of them, that is, antibodies targeting the CTLA-4 receptor of T cells and antibodies to the programmed death-1 receptor (PD-1), meanwhile belong to the first-line standard of care for the treatment of disseminated melanomas in patients who do not carry the BRAF[V600E] mutation.[13] However, although generally promising, this approach only induced long-lasting remission in a minority of patients,[14] while a substantial portion of patients poorly responded to the immunotherapy or did not respond at all. The reasons for the unresponsiveness are versatile, but the strong immunosuppressive TME appears to play a substantial role (reviewed in Byrne et al.[7] and Márquez-Rodas et al.[15]). Thus, melanoma still remains a difficult to treat tumor type and we are in urgent need to develop novel curative strategies.

It is increasingly being recognized that combining cancer treatments with different mechanisms of actions that have only moderate efficiencies in stand-alone application may lead to an additive or even synergistic anti-tumor effect. In pre-clinical studies, combination therapy of locally applied oncolytic reovirus and anti-PD-1 blockade on cytotoxic T cells resulted in enhanced oncolysis of melanoma cells compared to single applications of either reovirus or PD-1 blockade alone.[16] In agreement with these results, localized Newcastle disease virus (NDV) combination therapy with systemic CTLA-4 checkpoint blockade in pre-clinical melanoma *in vivo* models also showed promising synergistic effects.[17] Nevertheless, the remaining challenge is to therapeutically target lung-metastatic melanoma.

In this study, we sought to evaluate the oncolytic and immunomodulatory potential of intranasally applied IAV against melanoma lung metastases and to explore whether the initial IAV-induced oncolysis can be enhanced by combined application of IC inhibitors.

RESULTS

IAVs Efficiently Replicate in B16-F10 Melanoma Cells

For our studies, we employed the highly progressive B16-F10 melanoma cells. Being transplanted intravenously (i.v.) into syngeneic C57BL/6 mice, they readily colonize the lung tissue, imitating the formation of melanoma lung metastases.[18] To investigate whether this melanoma isolate is permissive for IAVs, B16-F10 cells were infected with different low and high pathogenic IAV strains (Figure 1A). All IAVs tested were able to infect and replicate in melanoma cells. Among IAVs with low pathogenicity (Figure 1A, left image), suitable as potential OVs, the recombinant A/Puerto Rico/8/34 (H1N1) (PR8) IAV showed the highest viral titers in melanoma cells. This virus strain is one of the best studied IAV strains and is in addition adapted to the mouse,[6,19,20] and it was therefore chosen for further experiments. Furthermore, the recombinant PR8 virus strain is a weak type I interferon inducer, and its replication is hardly affected by cellular innate immune response.[20] Infection of B16-F10 cells with PR8 IAV of different multiplicities of infection (MOIs) and for different time periods confirmed that B16-F10 cells can be readily infected with IAVs and that the production of viral progeny particles increases with time of infection, reaching a plateau at 36 h (Figure 1B). Furthermore, IAV infection and replication in B16-F10 cells proceed comparable to lung epithelial cells, which are their permissive target tissue. Upon viral replication, apoptotic marker gene expression is induced, and the infected cells undergo cell death in an MOI-dependent manner, as expected (Figures 1C and 1D).

B16-F10-Derived Lung Tumors Cause Local Immunosuppression

Prior to investigation of the oncolytic efficacy of IAV against B16-F10 lung metastases, we analyzed whether this type of tumor develops an immunosuppressive microenvironment and which type of immune
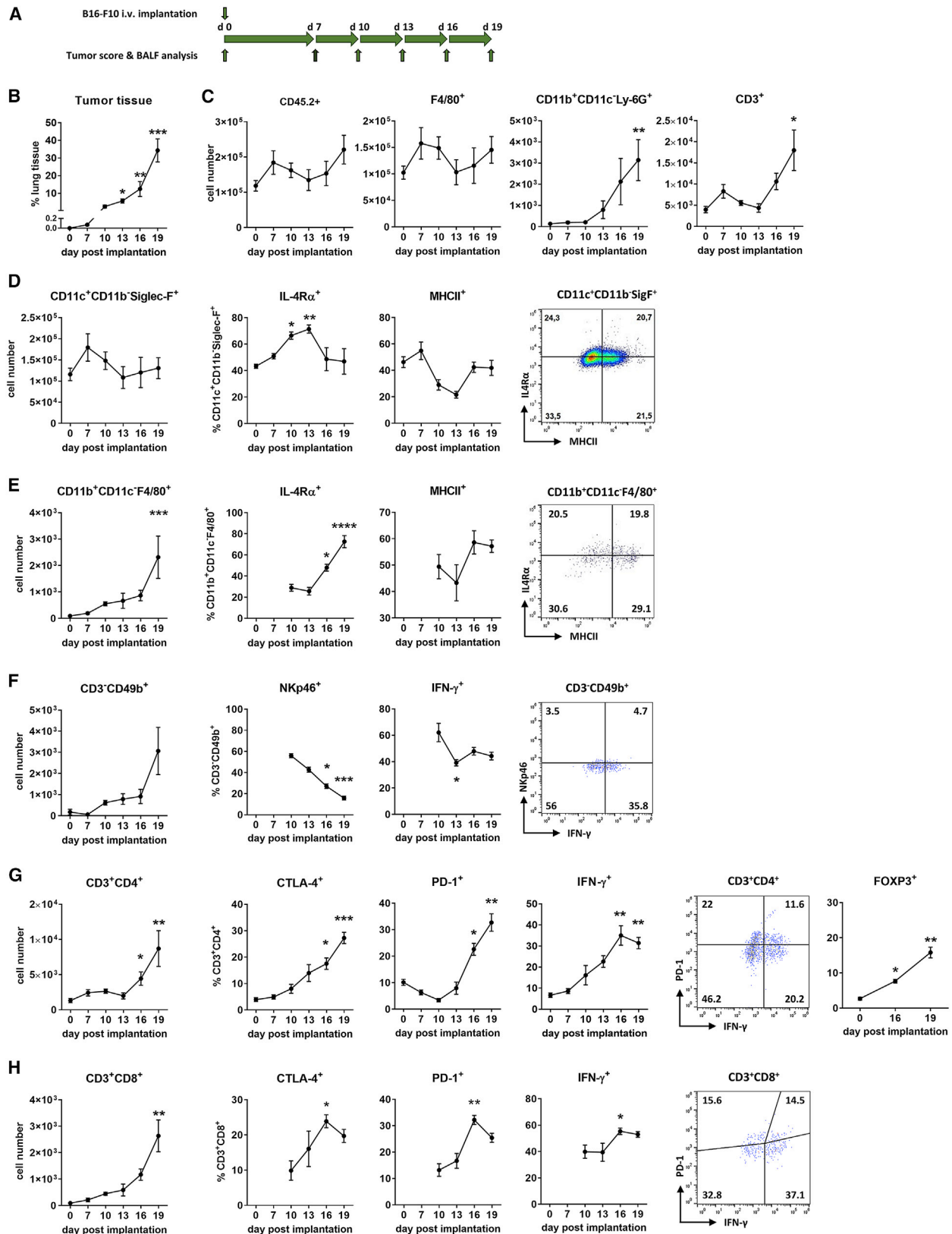
(legend on next page)

cells are attracted and affected by the progressively growing tumor. To track changes in lung immunity during growth of B16-F10 lung metastases, immune cells from bronchoalveolar lavage fluids (BALFs) of mice were analyzed by flow cytometry at different days after i.v. implantation of B16-F10 cells (Figure 2A; Figure S1). As expected, B16-F10 cells appeared as a highly aggressive tumor, which was evidenced by rapid increase in pulmonary tumor mass. The amount of melanoma-derived lung tumors, calculated as a ratio of the total lung tissue, increased from 0.07% of cancer tissue on day 7 to 34.3% on day 19 after implantation (Figure 2B). Tumor development was accompanied with only a slight increase of total lung immune cells, as judged by the amount of $CD45^+$ leucocytes in BALF (Figure 2C). Nevertheless, the composition of leucocytes changed upon progressive tumor growth. Most $CD45^+$ immune cells were represented by lung-resident alveolar macrophages ($CD45^+CD11c^+CD11b^-Siglec-F^+$), the amount of which did not change significantly but was always at least one order of magnitude higher than that of other immune cell populations analyzed (Figures 2C and 2D–2H, left panels).

Subsequent analysis of $CD45^+$ cells for other particular immune cell types revealed a significant attraction of neutrophils ($CD45^+$ $CD11b^+CD11c^-Ly-6G^+$), peripheral macrophages ($CD45^+CD11b^+$ $CD11c^-F4/80^+$), natural killer (NK) cells ($CD45^+CD3^-CD49b^+$), and T lymphocytes ($CD45^+CD3^+$), especially at late stages of metastatic growth (Figures 2C and 2E–2H, left graphs). Among immune cells that infiltrated into the lung during tumor progression, T lymphocytes represented the most abundant immune cell subtype. Their amount was roughly an order of magnitude higher than the levels of lung-infiltrating neutrophils, peripheral macrophages, or NK cells.

Although the total number of lung-resident alveolar macrophages ($CD45^+CD11c^+CD11b^-Siglec-F^+$) did not change significantly during progressive growth of B16-F10 metastases (Figure 2D, left graph), their characteristics underwent essential changes. They increasingly acquired an anti-inflammatory M2-like phenotype. Indeed, the proportion of cells expressing the anti-inflammatory interleukin (IL)-4 receptor alpha subunit (IL-4Rα) increased significantly, while the part expressing the basic activation and antigen-presentation marker major histocompatibility complex class II (MHCII) decreased,

showing an inverse kinetic compared to IL-4Rα-expressing cells (Figure 2D).

Interestingly, the lung-recruited peripheral macrophages were also polarized toward an M2-like phenotype. Similar to lung-resident macrophages, the number of IL-4Rα-positive cells increased with progressive growth of B16-F10 melanoma, reaching at day 19 of tumor growth roughly a 4-fold higher amount compared with cells derived from control lungs. The number of MHCII-positive peripheral macrophages also increased at early stages of progressive B16-F10 tumor growth, but stagnated almost completely at late stages (Figure 2E). Nevertheless, while showing some fluctuations, the levels of MHCII-positive peripheral macrophages did not change significantly upon progressive tumor growth.

NK cells, the innate immune cells with a cytotoxic effector function, were affected by the tumor as well. Being virtually undetectable in BALFs of control mice and of mice with small melanoma tumor size, they were continuously attracted to the lung with tumor growth progression (Figure 2F). However, they demonstrated a gradual decrease in the number of cells expressing the cytotoxicity receptor NKp46. The number of infiltrated NK cells able to produce the inflammatory cytokine interferon (IFN)-γ also decreased with progression of melanoma metastases, although to a lesser extent than NKp46-positive cells. Nevertheless, these data point toward a suppression of NK cells.

The number of adaptive immune cells, mostly represented by $CD45^+CD3^+$ T lymphocytes, continuously increased with tumor progression (Figure 2C). This increase was characteristic for both helper ($CD45^+CD3^+CD4^+$) and cytotoxic ($CD45^+CD3^+CD8^+$) T lymphocytes, although the content of T helpers in the BALF was more abundant compared to cytotoxic T cells (Figures 2G and 2H, left images). As in the case of NK cells, the $CD45^+CD3^+CD8^+$ cytotoxic T cells were virtually undetectable in lungs of mice shortly after tumor implantation, but their total numbers gradually increased during the progressive growth of B16-F10 metastases (Figure 2H). Interestingly, the number of immunosuppressive regulatory T (Treg) cells, the portion of FOXP3-positive cells among $CD3^+CD4^+$ T cells, also

Figure 2. Progressively Growing B16-F10 Pulmonary Metastases Cause Local Immunosuppression

(A) Schematic representation of the experimental setup of tumor score and BALF analysis after i.v. injection of syngeneic B16-F10 melanoma cells into C57BL/6 mice. (B) B16-F10 cells (2×10^5 per mouse) were injected intravenously to establish pulmonary metastases, and the amount of tumor tissue in relationship to total lung tissue was investigated via IHC staining of MCR1 at the indicated time points. Three histological lung specimen representing different lung parts were analyzed for each mouse. (C–H) Graphs represent changes in the immune status of the bronchoalveolar space of C57BL/6 mice after i.v. injection of 2×10^5 B16-F10 melanoma cells. (C) Absolute numbers of total leucocytes ($CD45.2^+$) as well as total numbers of macrophages ($F4/80^+$), neutrophils ($CD11b^+CD11c^-Ly-6G^+$), and T cells ($CD3^+$) as subpopulations of $CD45.2^+$ cells. For schematic representation of the principal gating strategy, see Figure S1. (D) Images represent alveolar macrophages ($CD11c^+CD11b^-Siglec-F^+$) in the BALF. The left image shows the total number of alveolar macrophages in BALF per mouse as part of $CD45.2^+$ cells. The middle images show the percentage of IL-R4α$^+$ and MHCII$^+$ cells. The right image is a dot plot distribution of these cells on day 19 after tumor implantation. The gating strategy by means of FMO controls is presented in Figure S2. (E) Images represent peripheral macrophages ($CD11b^+CD11c^-F4/80^+$). (F–H) Images represent (F) NK cells ($CD3^-CD49b^+$), (G) T helper cells ($CD3^+CD4^+$), and (H) T killer cells ($CD3^+CD8^+$) among $CD45.2^+$ cells in BALFs. As described for (D), the left images show the total number of appropriate cells per mouse, while the middle images show percentages of cells expressing indicated activation markers and the right images are dot plot distributions of cells with specific markers on day 19 after B16-F10 implantation. Note that the number of peripheral macrophages and NK cells in BALFs at early stages of tumor growth was very low, and no reliable data for cells expressing specific markers could be obtained. Data are expressed as means ± SEM, with n = 4-6 animals per group. *p < 0.05, **p < 0.01, ***p < 0.001 (Kruskal-Wallis test with a Dunn's multiple comparison test).

progressively increased with growing tumor mass (Figure 2G). Furthermore, the number of cells expressing IC receptors (CTLA-4 and PD-1) among both T helper and cytotoxic T lymphocytes gradually increased as well with progression of B16-F10 melanoma metastases growth, indicating an enhanced suppression of the adaptive immune response. Somewhat unexpected was the increased presence of IFN-γ-expressing T cells. Nevertheless, their levels stagnated at late stages of tumor progression (Figures 2G and 2H). Despite this seemingly activated state of infiltrating cytotoxic T cells, they were obviously not able to hinder the progressive growth of B16-F10 lung metastases (Figure 2B).

Taken together, these data demonstrate an increased infiltration of peripheral immune cells, but no changes in the absolute numbers of lung-resident alveolar macrophages. However, the amount of cells expressing anti-inflammatory marker proteins increased upon progressive cancer growth, indicating an accretive immunosuppressive TME and immune cell impairment. However, in advanced stages of cancer growth, the lung immune cell composition is highly heterogeneous, as flow cytometry analyses of pro-inflammatory and anti-inflammatory markers expressed by the respective immune cell subpopulations on day 19 of tumor growth showed (Figures 2D–2H, right graphs).

IAV Infection Promotes Destruction of B16-F10 Lung Tumors

Being encouraged by the highly efficient replication of IAV in B16-F10 cells *in vitro*, we wondered whether the progressive growth of B16-F10 lung metastases in syngeneic C57BL/6 mice can be reduced by IAV infection *in vivo*. Thus, mice bearing B16-F10 pulmonary metastases were infected with a sublethal dose of the low pathogenic recombinant PR8 IAV and analyzed for reduction of the number and size of metastatic foci. Based on the rapid and aggressive B16-F10 lung cancer growth (Figure 2A), mice were infected at day 7 after B16-F10 implantation (Figure 3A), a time point when metastatic foci have already been established but are still small in size, to enable unfolding of the acute IAV infection phase that usually lasts 9–10 days at the virus doses chosen.[6,20] On day 3 of infection, infected animals demonstrated significantly fewer numbers of surface metastases and a significantly reduced total tumor mass or size compared to mock-infected mice (Figures 3B and 3C). These data were further confirmed by qRT-PCR, demonstrating a reduced expression level of the melanocyte-specific gene dopachrome tautomerase (*Dct*) in lung tissue of IAV-infected compared to mock-infected mice at day 3 post-infection (p.i.) (Figure 3D). However, already at day 6 after infection, both the number of surface metastases and the size of tumor foci did not differ anymore between infected and mock-infected mice, and this trend kept unaltered until day 12 of infection, when the tumor mass reached an average of 34% of the total lung tissue (Figure 3C). Although the melanoma-specific *Dct* mRNA expression was always somewhat weaker in infected mice during the whole observation period, the levels also showed a significant difference between infected and mock-infected mice only on day 3 p.i. but not afterward, thus resembling the same tendency. Hence, IAV infection induced oncolysis of melanoma lung metastases, but the effect was not long-lasting.

To determine whether the short-lived oncolytic effect of IAV was a consequence of impaired viral replication in the lungs of cancer-bearing mice or the incapability of inducing long-lasting anti-cancer immune responses, we measured virus titers in BALF of control and tumor-bearing mice at different days of infection and analyzed the infected lung tissue by immunohistochemistry (IHC). Although virus titers varied between individuals, no significant differences in IAV replication between control and tumor-bearing mice could be measured for any of the analyzed time points (Figure 3E). Staining of infected lung tissue for viral nucleoprotein (NP) protein indicated viral infection of both healthy and tumor tissues (Figure 3F). Moreover, some infected tumor foci appeared as loosened structures without distinct boundaries in comparison with non-infected tumor foci. At day 6, however, the tumor foci showed a considerable increase in size with clear demarcation from healthy lung tissue and with NP-positive cells being localized mostly at the periphery of the dense foci structures but rarely inside of them, indicating that the extremely high proliferation capacity of B16-F10 cells (Figure 2B) might counteract oncolytic action of IAV.

IAV Infection of Cancer-Bearing Mice Resulted in Lung Infiltration by Immune Cells with an Activated Phenotype

To analyze whether the transient oncolytic effect of IAV infection is a result of an altered immune response in mice with B16-F10 metastases, BALF-derived immune cell subsets from control and tumor-bearing mice were compared for their absolute levels as well as for activation markers by flow cytometry at different time points after IAV infection. Data presented in Figure 4 show that both mouse groups responded roughly equally well to IAV infection. As typical for IAV-infected mice, the number of immune cells in BALF increased dramatically during the acute phase of infection, until day 9, and declined afterward when the clearance of IAV particles occurs.[19,20] As expected, neutrophils and peripheral macrophages showed their highest lung infiltration rate at day 3, NK cells at day 6, and T lymphocytes at day 9 p.i. (Figures 4A and 4C–4F, left images). Also predictable, the number of resident alveolar macrophages gradually reduced until day 9 (Figure 4B) due to apoptosis caused by IAV infection.[21] However, infiltration of tumor-bearing lungs with peripheral macrophages was somewhat more sustained compared to lungs of control mice (Figure 4C), and the amount of CD45$^+$CD3$^+$CD8$^+$ cytotoxic T cells was higher in mice with B16-F10 lung metastases (Figure 4F).

As expected after a strong acute immune response, the number of IL-4Rα-positive macrophages, of both alveolar and peripheral subtypes, increased to limit a profound inflammatory response.[22] The levels of MHCII-positive alveolar and peripheral macrophages increased as well, indicating that IAV infection activated this type of immune cells in both groups of mice (Figures 4B and 4C). NK cells were also strongly attracted to infected lungs and showed a high proportion of activated cells, as judged by expression of NKp46 and IFN-γ (Figure 4D).

Likewise, the number of adaptive T helper cells (CD45$^+$CD3$^+$CD4$^+$) and cytotoxic T cells (CD45$^+$CD3$^+$CD8$^+$) increased strongly in
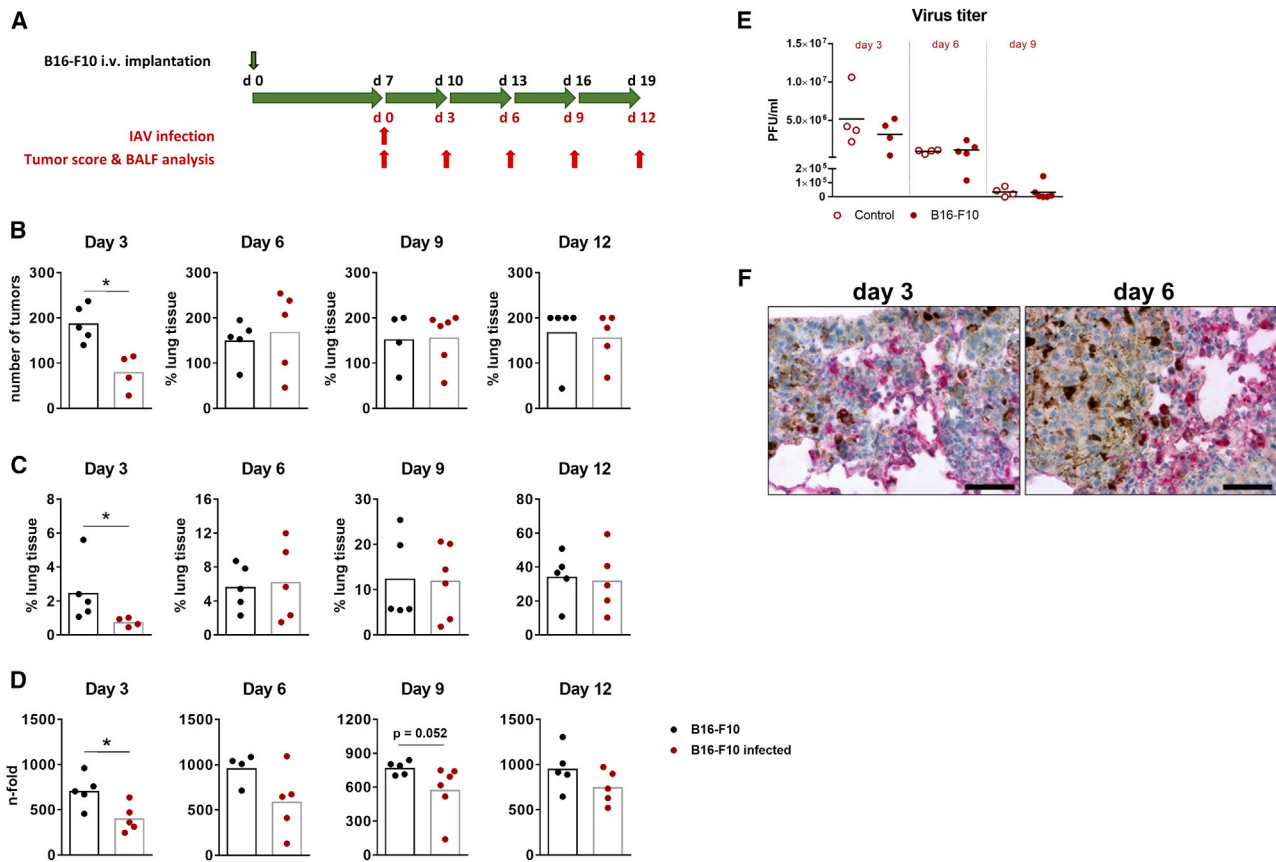
Figure 3. IAV Infection Mediates Oncolysis of B16-F10 Melanoma Lung Metastases

(A) Schematic representation of IAV infection, tumor score, and BALF analysis of C57BL/6 mice after i.v. injection of syngeneic B16F10 melanoma cells. (B–D) B16-F10 cells (2×10^5 per mouse) were injected intravenously to establish pulmonary metastases. After 7 days, animals were infected with 300 plaque-forming units (PFU) of influenza A/PR8/8/34 (PR8) H1N1 strain (red symbols) or mock-infected with PBS (black symbols) and the lung tumor burden was determined each third day after infection. (B) Numbers of tumor foci on the surface of right lungs at indicated days after IAV infection. (C) Content of tumor tissue in lungs was calculated as a ratio of MC1R-positive tumor area normalized to the whole-lung section area after different days of IAV infection. (D) The expression of melanoma-specific *Dct* mRNA in lung tissues was measured by TaqMan qRT-PCR. The values are normalized to *Dct* mRNA levels of control animals that had not been injected with B16-F10 cells or infected with PR8. (E) Control (open symbols) or B16-F10-implanted (filled symbols) mice were infected with 300 PFU of PR8 IAV, and virus titers in BALFs were determined by plaque assay at times indicated. Values of individual animals and mean values (black lines) per group are shown. (F) Paraffin lung sections of tumor-bearing mice infected for 3 or 6 days with PR8 IAV were stained for expression of viral NP protein (red) and counterstained with hematoxylin (blue). Most melanoma cells show characteristic melanin inclusions. Scale bars, 50 μm. *$p < 0.05$, **$p < 0.01$, ***$p < 0.001$ (B–D, Mann-Whitney U test; E, two-way ANOVA followed by Sidak's multiple comparisons test)

BALF in both control and tumor mice, reaching the maximum at day 9 after IAV infection (Figures 4E and 4F). Both types of T cells were increasingly activated according to increasing expression of IFN-γ. The number of CTLA-4- and PD-1-positive cells among helper and cytotoxic T cells also rose, indicating that IAV infection induced a strong acute immune response and additionally emphasizing the activation of feedback mechanisms to prevent a too profound inflammatory response.[23,24] Of note, while the number of IFN-γ-positive $CD3^+CD4^+$ T cells constantly increased after IAV infection in mice with lung metastases, the number of immunosuppressive $CD3^+CD4^+$ Treg cells decreased (Figure 4E). They represented only 4.5% and 3.8% of the total $CD3^+CD4^+$ T cell population at day 9 and 12 of infection, respectively. In non-infected tumor-bearing mice these numbers were 9.0% and 12%, accordingly. In non-tu-

mor-bearing control mice, the proportion of Treg cells increased after IAV infection in the course of the restricting feedback mechanism, but only slightly, being represented by 2.7% in non-infected lungs to 3.3% and 3.4% in 9- and 12-day-infected mice, respectively.

Interestingly, higher levels of cytotoxic $CD3^+CD8^+$ T lymphocytes infiltrated the infected lung when melanoma metastases were present, even though viral replication did not differ in these mice compared with control non-tumor-bearing animals. Nevertheless, the infiltration pool of these cells decreased massively in mice with tumors after day 9 of infection, while in control non-tumor mice it was kept at a high value until day 12 p.i. Of note, at day 9 of infection, or day 16 of B16-F10 transplantation, the tumor mass expanded dramatically (Figure 2B).
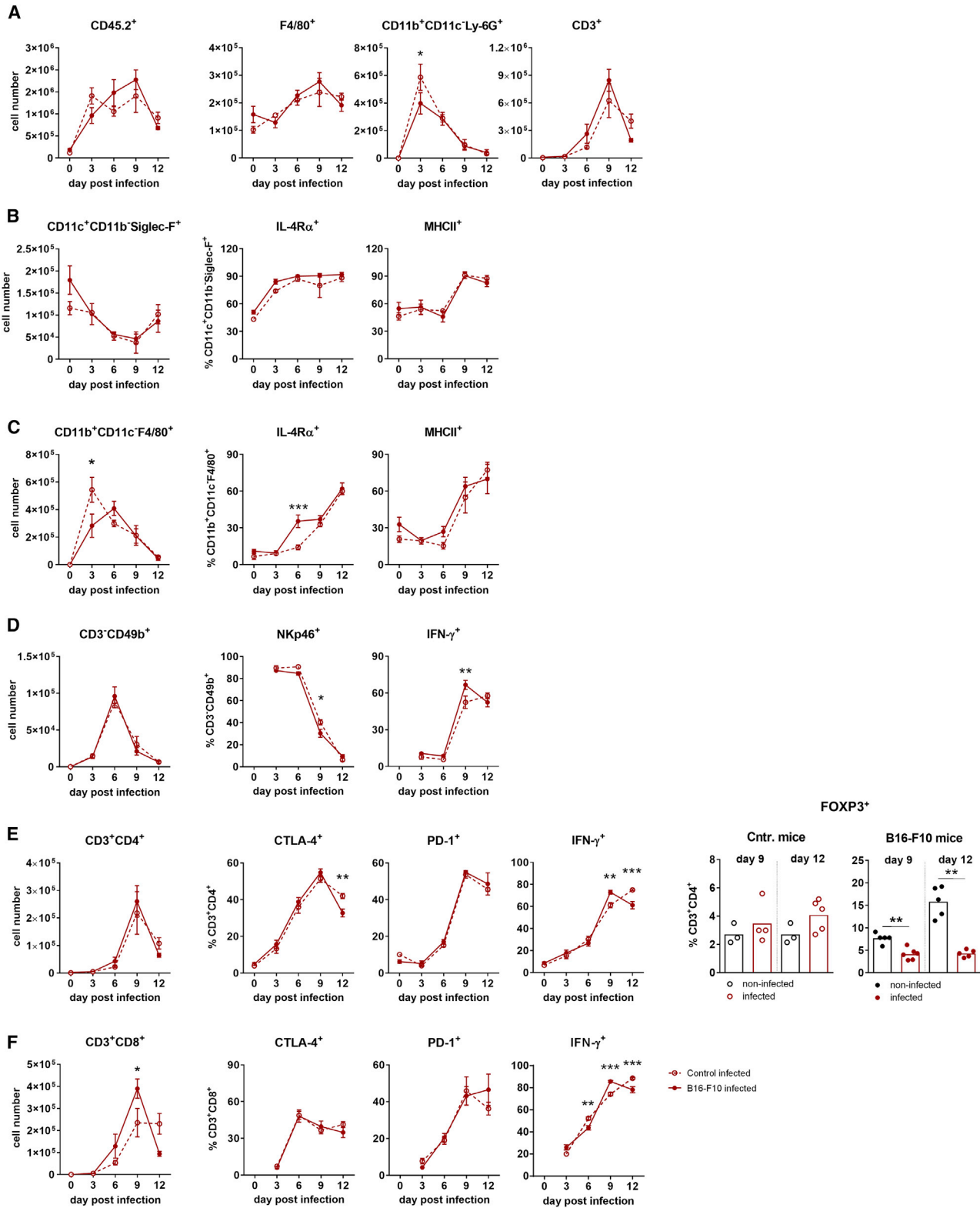
(legend on next page)

In summary, the presence of lung melanoma metastases did not alter the overall innate and adaptive immune response to IAV infection. Both kinetics and intensities of immune responses developed in a similar way. Remarkably, IAV infection of tumor-bearing mice abrogated the existing immunosuppressive state almost completely. Indeed, a significant decrease in Treg cells and a strong increase in peripheral macrophages, NK cells, and T cells expressing pro-inflammatory marker proteins could be detected. Finally, in light of these data, it was rather unexpected that IAV infection induced only a transient oncolytic effect and that the IAV-induced immune responses were not capable of provoking long-lasting anti-cancer lytic efficacy.

PD-1 Blockade Improves Oncolytic Effect of IAV Infection
Next, we wondered whether augmentation of the immune response that has been developed to oncolytic IAV infection could convert the transient oncolysis of lung melanoma metastases into a persistent action. Inhibition of IC receptors or ligands seems to be a suitable strategy to provoke sustained action, particularly as this approach is currently one of the most effective treatments of advanced melanoma. Thus, we searched for potential IC targets on B16-F10 cells and revealed a high expression of PD-1 ligand 1 (PD-L1) and B7-H3 IC ligands (Figure 5A). Based on these results and on strong expansion of PD-1^{+} T lymphocytes upon progressive cancer growth *in vivo* (Figures 4E and 4F), we decided to combine IAV infection with suppression of PD-1 signaling.

To this end, mice with pulmonary B16-F10 metastases were infected with a sublethal dose of PR8 virus and additionally subjected to therapy with anti-PD-1 monoclonal antibodies (mAbs), each on the third day after infection. The anti-tumor effect was analyzed at day 12 p.i. or after triple antibody injection (Figure 5B). The experimental setup is based on the experimental design published by Rojas et al.,[25] who found that tumor cell lysis and release of tumor-associated antigen (TAAs) should precede the IC inhibitor implementation. A 3-day delay in immunotherapy after infection onset provides sufficient virus replication (Figure 3E) and development of immune response (Figure 4). Data presented in Figure 5C show that application of anti-PD-1 mAb alone was not able to disturb the progressive growth of B16-F10 metastases, but its combination with IAV infection resulted

in roughly a 50% reduction of both surface tumors and the tumor mass (Figure 5C).

In good agreement with these results, application of anti-PD-1 mAb resulted in increased secretion of pro-inflammatory cytokines only when combined with IAV infection (Figure 5D). Nevertheless, application of PD-1 antibody resulted in reduced levels of PD-1 positively stained T lymphocytes in both non-infected and IAV-infected mice (Figures 6E and 6F), supporting the functionality of the antibody used. Interestingly, however, the anti-PD-1 mAb did not influence any of the analyzed immune cell population in non-infected tumor-bearing mice, except the Treg cells, whose number was reduced (Figure 6E).

In sharp contrast, administration of the anti-PD-1 mAb in addition to IAV infection led to increased infiltration of immune cells into lungs, including peripheral macrophages, neutrophils, NK cells, and helper and cytotoxic T lymphocytes (Figure 6). The number of lung-resident alveolar macrophages surprisingly decreased strongly upon combinational treatment (Figure 6B). The reasons for this phenomenon are still unclear. The number of Treg cells already reduced by IAV infection was not further reduced in this mouse group by anti-PD-1 mAbs (Figure 6E). Interestingly, although the number of immune cells attracted into infected lungs was increased after anti-PD-1 mAb application, the relative amount of immune cells that were already activated by IAV infection did not change for most of the cell types analyzed (Figure 6). In summary, data from this experiment show that application of anti-PD-1 mAb along with IAV infection results in significant reduction of B16-F10 metastases and that inhibition of the PD-1/PD-L1 axis synergizes in action with the immune response to IAV infection, resulting in enhanced immune cell recruitment to the tumor site.

DISCUSSION
In this study, we show that progressively growing B16-F10 melanoma lung metastases attract different types of immune cells, including neutrophils, peripheral macrophages, NK cells, and T cells. These cells, however, display an immunosuppressed inactive phenotype. We further demonstrate that mice with B16-F10 lung metastases react

Figure 4. Immune Status of the Bronchoalveolar Space of Control Mice and Mice with B16-F10 Melanoma Lung Metastases after Infection with PR8 Influenza Virus

Control (dashed lines, open symbols) and tumor-carrying (lines, filled symbols) mice were infected and analyzed according to the schedule shown in Figure 3A, and the lung immune status was analyzed by flow cytometry of BALF containing cells. (A) Absolute numbers of total leucocytes (CD45.2^{+}) as well as total numbers of macrophages (F4/80^{+}), neutrophils (CD11b^{+}CD11c^{−}Ly-6G^{+}), and T cells (CD3^{+}) as parts of CD45.2^{+} cells. For principal gating strategy, see Figure S1. (B) Images represent alveolar macrophages (CD11c^{+}CD11b^{−}Siglec-F^{+}) in the BALF after IAV infection. The left image shows the total number of alveolar macrophages as part of CD45.2^{+} cells in BALF per mouse. The middle and right images show the percentage of IL-R4α- and MHCII-positive alveolar macrophages. (C) Infiltration kinetics of the BAL space by peripheral macrophages (CD11b^{+}CD11c^{−}F4/80^{+}), with the left image showing the total amount of cells per mouse and the middle and right images showing percentages of IL-R4α- and MHCII-positive cells. (D) Infiltration kinetics of the BAL space by NK cells (CD3^{−}CD49b^{+}), with the left image showing the total amount of NK cells per mouse and the middle and right images showing percentages of NK cells expressing the activation markers NKp46 and IFN-γ. (E and F) Infiltration kinetics of BAL space by (E) T helper (CD3^{+}CD4^{+}) and (F) T killer (CD3^{+}CD8^{+}) cells, with the left image showing the total amount of appropriate cell population per mouse and other images showing T cell populations expressing activation markers CTLA-4, PD-1, and IFN-γ. The right images of (E) show percentages of FOXP-positive Treg cells in BALF of control and tumor-containing mice at day 9 and 12 after IAV infection in comparison to their non-infected counterparts. Note that the number of NK and T killer cells in BALFs of non-infected mice was too low to obtain reliable data for cells expressing specific markers. Data are expressed as means ± SEM, with n = 4–6 animals per group. *p < 0.05, **p < 0.01, ***p < 0.001 (Kruskal-Wallis test with Dunn's multiple comparison test).
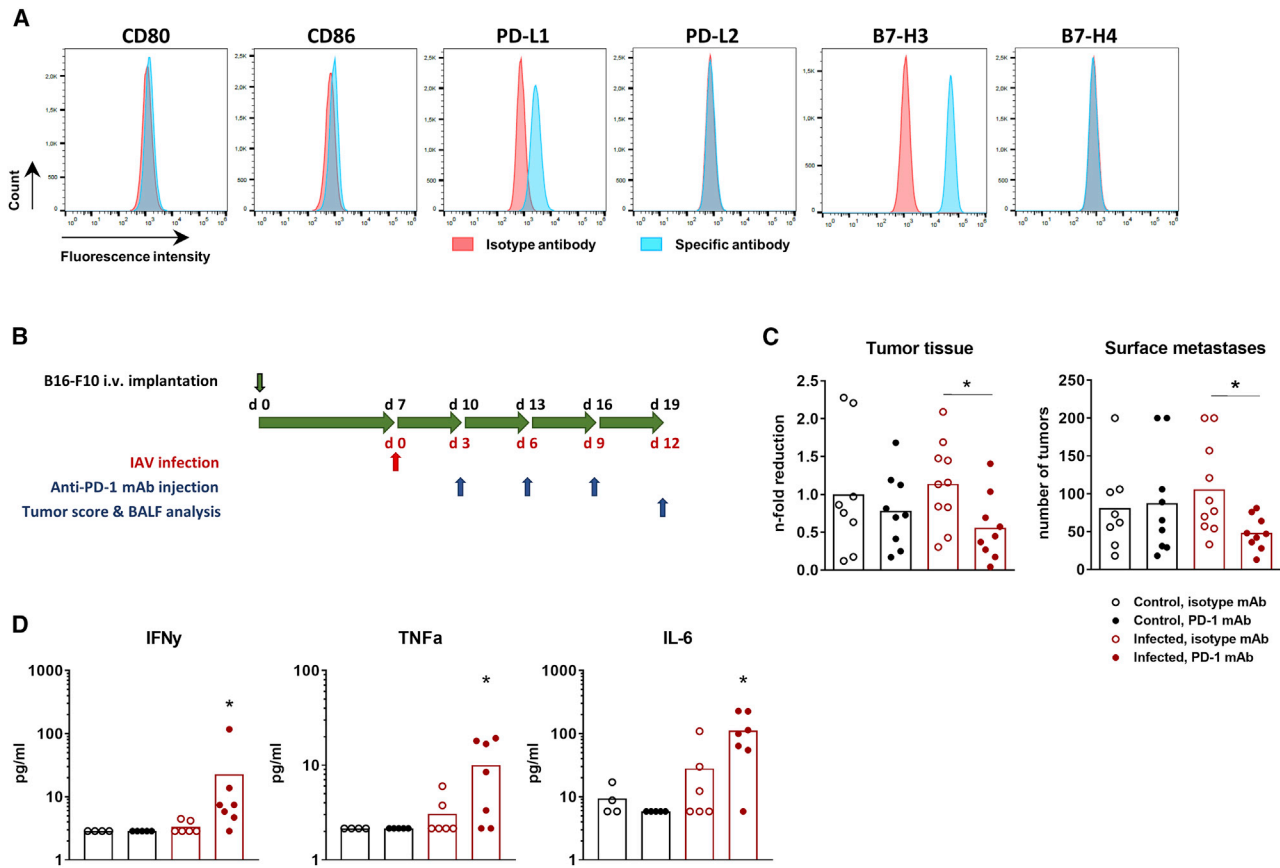
Figure 5. PD-1 Blockade Enhances IAV-Mediated Oncolysis of B16-F10 Melanoma Lung Metastases

(A) Immune checkpoint profile of B16-F10 cells. *In vitro*-cultivated B16-F10 cells were subjected to flow cytometry analysis for different IC molecules, including CTLA-4 ligands CD80 and CD86, PD-1 ligands PD-L1 and PD-L2, as well as B7-H3 and B7-H4. Shown are FACS histograms representative of two independent experiments. (B) Time schedule of IAV infection (red arrow), anti-PD-L1 mAb injections, tumor score, and BALF analysis (blue arrows) of C57BL/6 mice after i.v. injection of syngeneic B16F10 melanoma cells (upper black arrow). (C) The number of surface metastases and their progressive growth were calculated on day 12 p.i. as described in the legend of Figure 3. The amount of tumor tissue in non-infected mice treated with the isotype antibody was assigned a value of 1 (right image, black column with open symbols). Values of individual animals and mean values (columns) per group are shown. *p < 0.05 (one-way ANOVA followed by Dunnett's multiple comparison test). (D) Levels of pro-inflammatory cytokines in BALFs were measured on day 12 p.i. Values of individual animals and mean values (columns) per group are shown.

to IAV infection with an even partly stronger response than do control mice, simultaneously abrogating the immunosuppressed phenotype of tumor-associated macrophages and lymphocytes. Furthermore, infection of mice with B16-F10 lung metastases with sublethal doses of IAV results in a more than 50% reduction in the number and size of metastatic foci. However, the effect reached a maximum on day 3 p.i. but was not long-lasting. Finally, application of anti-PD-1 mAbs, which did not exhibit effects in stand-alone application, had a sustained effect on lung metastases when applied in combination with IAV infection, delaying their growth by 50% at late stages of tumor progression.

Despite the great progress made in treatment of malignant melanoma in the last 30 years, the management of disseminated unresectable metastases still represents an arduous challenge. In addition to targeted chemotherapy, application of OVs and immunotherapy are increasingly acknowledged among current strategies against this type of cancer. Melanomas carrying the BRAF[V600E] mutation can be efficiently treated with BRAF inhibitors (vemurafenib, dabrafenib) and their combination with the MEK inhibitor trametinib results in an extended therapeutic window and delays development of resistance.[26] Alternatively, this approach is not suitable for tumors with non-mutated BRAF kinase where it promotes an accelerated tumor progression as a result of paradoxical BRAF activation (reviewed in Lito et al.[27]). Oncolytic virotherapy of melanoma patients is limited so far to talimogene laherparepvec (T-VEC) virus, which is at present the most clinically advanced OV for primary melanoma. However, there is no evidence that T-VEC treatment leads to reduction of melanoma metastases in visceral organs or extends survival of patients with such a disease progression (reviewed in Bommareddy et al.[28] and Johnson et al.[29]). In the present study, we used oncolytic IAV to specifically target melanoma-derived lung metastases. The
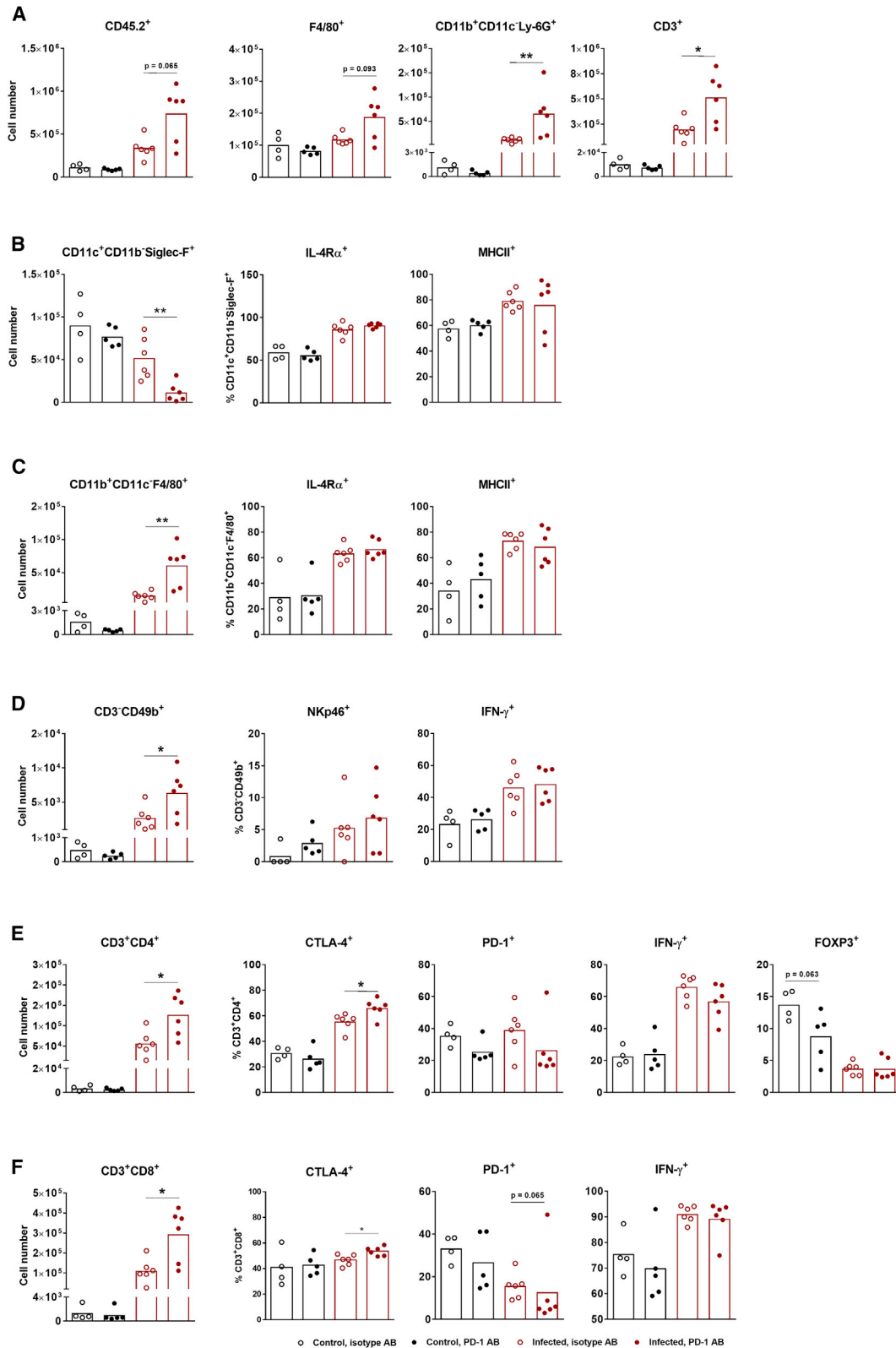
(legend on next page)

rationale of this strategy is based on the fact that lung tissue is readily accessible by IAVs and that many melanoma cells, including the mouse B16-F10 cells used in this work, are highly permissive for IAVs (Figure 1).[12] IAVs, or the related respiratory virus Newcastle disease virus, have already been used in animal research as anti-melanoma agents, but only for intratumoral injection of subcutaneously growing tumors, which were effectively reduced in their growth.[11,17] In this study, we showed for the first time that IAVs are also effective against melanoma metastases that have spread in the lung and are not accessible for intratumoral OV delivery. Moreover, our results demonstrate that IAV infection of mice with B16-F10 lung metastases leads not only to a direct oncolytic effect but also to a strong antiviral response and abrogation of tumor-mediated immunosuppression. Both innate and adaptive immune cells restored their functional immune phenotype. The infiltration of lungs containing melanoma metastases with adaptive CD3+CD8+ cells after IAV infection was even stronger than that in control mice. This effect, however, faded out at late stages of tumor growth, probably due to the extremely high progression of metastases at this stage.

B16-F10 melanoma is an extremely aggressive neoplasm, and although i.v. implantation of B16-F10 cells does not represent the full substantial changes that primary cancer cells undergo upon metastasis formation and lung implantation, this syngeneic experimental model is the most commonly used metastatic melanoma model for preclinical studies.[18,30] Being injected i.v., B16-F10 cells readily attach to lung tissue and form numerous tumor foci that grow very rapidly, killing mice during 3–4 weeks at the doses used in this work (Figure 2B).[18,30] The number of tumor foci in the lung was already high at day 7 after i.v. transplantation and remained virtually unchanged until day 19. Only their size increased rapidly, particularly during the late stage of progression (Figures 2B and 3B–3D). The tumor tissue can occupy up to one third of the lung tissue at day 19 after inoculation. This extremely strong progressive growth was probably the reason for the only transient oncolytic effect observed, despite the facts that the size of melanoma metastases at the time of infection was below 1% of the total lung tissue mass, the oncolysis was considerably efficient, reaching more than 50% of tumor reduction, and that IAV infection abrogated the tumor-mediated immunosuppression. In general, infection of lungs with IAVs is also a transient and self-limiting event. Even in the case of infection with replication-competent viruses at sublethal doses, IAV lung infection is usually cleared by day 9–10 p.i.[19,20,31] In addition, the lung tissue is never infected comprehensively. Even when high virus doses are used and the virus solution is dispersed as an aerosol directly into trachea, not all lung cells are infected and virus propagation still remains patchy.[6,32] Results of this work demonstrate that in the case of tumors with high oncogenic progressive growth, the amount of remaining non-lysed cells is obviously enough to overcome the oncolytic effect induced by such a strong infection as used in the present work. Indeed, this was not the case with slowly growing mouse NSCLC transformed by Raf oncogene.[6] In the present study, a sublethal infection with IAV resulted in a long-lasting oncolytic effect that was also spread over non-infected lung areas by tumor-infiltrating immune cells with restored immunocompetence.

The presence of tumor-associated immune cells in high quantities is generally a good prognostic factor and gives a chance to modulate their tumor-supporting and immunosuppressed phenotype toward tumoricidal activity by means of viral infection or ICI. IAV infection of mice carrying B16-F10 lung metastases indeed caused a significant reduction of tumor load early after virus challenge (Figure 3) but not after later stages of IAV infection. Hence, to enhance the short-term IAV-initiated oncolytic effect, mice with B16-F10 lung metastases were additionally treated with IC inhibitors. Both animal research and clinical trials during the last decade increasingly recognized the perspectives of combined therapeutic approaches, especially for tumors, which are difficult to target therapeutically. Regarding IC inhibitors, successful application of CTLA-4 and PD-1 inhibitors revolutionized strategies to cure patients with advanced inoperable melanoma. However, substantial numbers of patients do not demonstrate a stable response to currently available ICI methods and therefore require additional therapies. Poor sensitivity to CTLA-4 and PD-1 inhibition is related to low expression of these IC molecules by immune cells, low expression of the MHCI complex by melanoma cells, and weak tumor infiltration with T lymphocytes (reviewed in Byrne et al.[7] and Márquez-Rodas et al.[15]).

IAV infection of mice with B16-F10 lung melanoma metastases caused an increase in the content of T cells expressing CTLA-4 and PD-1 receptors (Figures 4E and 4F) as a natural mechanism of counteracting host immune response,[23,24] and thus increased their sensitivity to the IC blockade. This fact prompted us to target the PD-1/PD-L1 signaling axis. The monotherapy with anti-PD-1 antibody was, similar to IAV infection only, not able to induce sustained tumor regression. However, the combination of these two methods synergistically enhanced the immune response (Figure 6) and led to a significant decrease of melanoma tissue at advanced stages of B16-F10 growth, i.e., day 19 after tumor cell implantation (Figure 5). Although the effect of the combined therapy was obvious, it did not provide a radical melanoma cell elimination, indicating that different application schedules or other approaches are needed. In case of combined

Figure 6. PD-1 Blockade Enhances the Immune Response of Melanoma-Bearing Mice to IAV Infection

C57BL/6 mice were i.v. injected with B16-F10 cells to establish pulmonary metastases and infected with IAV with following subjection to an immune checkpoint inhibitor according to the schedule shown in Figure 5B. At day 12 post-infection, the lung immune status was analyzed by flow cytometry of BALF containing cells. (A and left images of B–F) Absolute numbers of (A) total leucocytes (CD45.2+) as well as total numbers of macrophages (F4/80+), neutrophils (CD11b+CD11c−Ly-6G+), T cells (CD3+), (B) alveolar macrophages (CD11c+CD11b−Siglec-F+), (C) peripheral macrophages (CD11b+CD11c−F4/80+), (D) NK cells (CD3−CD49b+), (E) T helper cells (CD3+CD4+), and (F) T killer cells (CD3+CD8+) among CD45.2+ cells in BALFs. (B–F, right images) Immune cells expressing specific markers are shown as percentages of the respective cell types. Values of individual animals and mean values (columns) per group are shown. *p < 0.05, **p < 0.01 (Mann-Whitney U test).

therapy, the "first anti-tumor hit" by OVs seems to be of special importance. Ideally, it should eliminate the vast majority of tumor cells and reverse the immunosuppression of the tumor-associated immune cells. IAV infection of B16-F10 melanoma-bearing mice could not fulfill these criteria to the full extent. Nevertheless, these data underscored the reasonableness of performing phenotypic analysis of cancer cells and tumor-associated immune cells prior to immunotherapy. It allows identifying the best suitable targets to maximize chances of positive response to the primary hit and the IC blockade for distinct individuals. The list of newly discovered IC pathways as well as recently developed antibodies for their inhibition is growing, which opens additional perspectives for patient-specific treatment.

In conclusion, we have demonstrated that IAV infection of mice with progressively growing melanoma lung metastases promotes a significant oncolysis and abrogates the tumor-mediated immunosuppression of infiltrated immune cells. We further demonstrated that while IAV infection and inhibition of the PD-1/PD-L1 IC signaling axes were rather inefficient in a long-lasting prevention of the progressive growth of melanoma-derived lung cancers when applied separately, their combined application led to significant sustained growth retardation of metastases.

MATERIALS AND METHODS
Ethics Statement
All experiments were performed with 2- to 4-month-old C57BL/6 mice of both sexes. Animals were kept under pathogen-free conditions. Experiments were planned and performed according to the German regulations of the Society for Laboratory Animal Science (GVSOLAS) and the European Health Law of the Federation of Laboratory Animal Science Associations (FELASA). Experimental protocols were approved by the Landesamt für Natur, Umwelt und Verbraucherschutz Nordrhein-Westfalen (LANUV-NRW), Germany.

In Vitro Infection of B16-F10 Cells
Murine melanoma B16-F10 cells were purchased from ATCC (catalog no. CRL-6475) and propagated in Dulbecco's modified Eagle's medium (DMEM; Merck, Darmstadt, Germany) supplemented with 10% heat-inactivated fetal bovine serum (FBS; Biochrom, Berlin, Germany). To avoid a random drift and selection of particular clones, cells were only used at passages two to five.

For analysis of IAV replication, B16-F10 cells were infected with the indicated MOI of recombinant low pathogenic human influenza strains A/Puerto Rico/8/34 (PR8; H1N1), A/WSN/1933 (WSN; H1N1), or A/Victoria/75 (Victoria; H3N2), as described before.[33] Despite that, B16-F10 cells were infected with the highly pathogenic avian influenza a virus isolates A/Thailand/KAN-1/2004 (KAN-1; H5N1) and A/FPV/79/Bratislava (fowl plague virus; H7N7) under biosafety level 3 (BSL-3) conditions. Viruses were propagated on Madin-Darby canine kidney (MDCKII) cells cultured in minimum essential medium (MEM; Merck, Darmstadt, Germany) containing 10% FBS. After designated time points, cell medium was collected for a standard plaque assay[34] to determine the numbers of infectious

viral particles. Virus titers are expressed as plaque-forming units (PFU) per mL.

To determine the portion of dead or apoptotic sells after IAV infection, B16-F10 cells were either stained with fixable viability dye eFluor 450 (eBioscience, Frankfurt, Germany) to evaluate percentage of dead cells via flow cytometry (Gallios, Beckmann Coulter, Krefeld, Germany) or RNA was isolated for subsequent mRNA gene expression analysis by qRT-PCR.

Animal Experiments
For tumor challenge experiments, B16-F10 cells (2×10^5) were injected into the lateral tail vein of C57BL/6 mice in a total volume of 100 μL of PBS to establish tumor foci growth in the lungs. Control mice were injected with 100 μL of PBS. One week later and every 3 following days until day 19, groups of mice were euthanized and BALF was collected to obtain lung immune cells as described earlier.[19] Afterward, lungs were extracted, the left lung was used for total RNA isolation, and the right lung was processed for IHC staining. Prior to IHC processing, the number of B16-F10 tumor foci on the surface of the right lung was evaluated macroscopically.

For IAV infection, control or tumor-bearing mice were anesthetized and 50 μL of viral stock solution in PBS was administered intranasally. All infection experiments were performed with 300 PFU of the recombinant influenza virus strain A/Puerto Rico/8/34 (PR8, H1N1). At this dose of PR8 virus, all mice, both control and melanoma-bearing mice, survived the infection. Typically, they started to loose body weight at day 3 of infection, but recovered again beginning at day 7–8 p.i.[6,19,20] The health status of infected animals and body weight loss were monitored daily.

On designated days, mice were euthanized and processed according to experimental schedules shown in Figures 3A and 5B. The number of infectious virus particles in the BALF was determined by standard plaque assay and viral titers were expressed as PFU/mL.[34] For PD-1 blockade, mice were receiving intraperitoneal injections of 250 μg of anti-PD-1 antibody (clone 29F.1A12) or of anti-trinitrophenol antibody as isotype control (Bio X Cell, West Lebanon, NH, USA).

RNA Isolation and qRT-PCR
RNA from infected B16-F10 cells was isolated using an RNeasy kit (QIAGEN, Hilden, Germany). Left mouse lungs were collected at indicated time points, and total lung RNA was isolated using peqGOLD TriFast reagent (VWR, Darmstadt, Germany). Samples were homogenized (FastPrep-24 homogenizer, MP Biomedicals, Eschwege, Germany) and total RNA was isolated via phenol/chloroform extraction and isopropanol precipitation. The precipitated RNA was then purified in a secondary phase separation step as previously described.[35] Obtained RNA was reverse transcribed into cDNA using the a high-capacity cDNA reverse transcription kit (Thermo Fisher Scientific, Schwerte, Germany) according to the manufacturer`s protocol. Levels of mRNAs were determined by TaqMan qRT-PCR on a LightCycler 480 II machine (Roche, Mannheim, Germany) using

Table 1. Oligonucleotides Used for qRT-PCR

Gene	Primers	Universal Probe (Roche)
Cytochrome c	5′-GCTACCCATGGTCTCATCGT-3′ 5′-GAAACCCCTCCGAATGCT-3′	#55
Dct	5′-GGCTACAATTACGCCGTTG-3′ 5′-CACTGAGAGAGTTGTGGACCAA-3′	#6
Fas	5′-AAACCAGACTTCTACTGCGATTCT-3′ 5′-GGGTTCCATGTTCACACGA-3′	#76
GAPDH	5′-TGTCCGTCGTGGATCTGAC-3′ 5′-CCTGCTTCACCACCTTCTTG-3′	#80
Tnfsf10	5′-GCTCCTGCAGGCTGTGTC-3′ 5′-CCAATTTTGGAGTAATTGTCCTG-3′	#76

oligonucleotides listed in Table 1. Each cDNA sample was analyzed in duplicate and specific signals were normalized to the signal of the housekeeping gene transcript cytochrome c (Cycs) for Dct or GAPDH for Fas (Fas cell surface death receptor) and Tnfsf10 (tumor necrosis factor-related apoptosis-inducing ligand, TRAIL). Sequences of primers used for qRT-PCR are listed in Table 1.

Analysis of Lung Immune Status

To collect lung immune cells, BAL was performed as previously described.[20] Briefly, mice were euthanized, the trachea was exposed, and the lungs were washed four times with 800 μL of PBS containing 2 mM EDTA. Supernatants of the first lavage were kept separately for viral plaque titration, a lactate dehydrogenase assay, and analysis of cytokine quantities in BALF. Cell pellets of the first lavage were combined with cells of the following lavages and centrifuged at $400 \times g$ for 10 min at 4°C. Erythrocytes were lysed, cell numbers were determined, and equal amounts of cells were subsequently stained for flow cytometric analysis (Gallios, Beckman Coulter; FACSCalibur, Becton Dickinson, Heidelberg, Germany).

Prior the specific staining, non-specific binding of antibodies was blocked by incubation with anti-CD16/CD32 antibody (BD Pharmingen, Heidelberg, Germany). Extracellular staining of cells was performed by incubation of cells with appropriate fluorochrome-labeled antibodies for 30 min at 4°C in the dark. Subsequently, samples were washed with PBS and then fixed and permeabilized for staining of intracellular proteins using the eBioscience Foxp3/ transcription factor staining buffer set (Thermo Fisher Scientific, Schwerte, Germany). Afterward, staining for intracellular proteins was performed as previously described.[36] Fluorescently labeled antibodies used for staining are listed in Table 2. Analysis of fluorescence-activated cell sorting (FACS) results was done using FlowJo software v10 (Becton Dickinson, Ashland, OR, USA) and was based on the fluorescence minus one (FMO) strategy as indicated in Figure S2. The principal gating strategy for the respective immune cell subsets is shown in Figure S2. The total numbers of immune cells were determined by gating on single cell subsets, followed by normalization to the absolute number of cells counted in the BALF of each individual mouse.

Table 2. Antibodies Used for Low Cytometry Analysis

Marker	Fluorophore	Clone	Manufacturer
B7-H3	APC	MIH35	BioLegend
B7-H4	PE	HMH4-5G1	BioLegend
CD11b	Pacific Blue	M1/70	BioLegend
CD11c	PE/Dazzle 594	N418	BioLegend
CD16/CD32	–	2.4G2	BD Pharmingen
CD3	PE/Cy7	145-2C11	eBioscience
CD3	PE/Dazzle 594	145-2C11	BioLegend
CD4	APC/Fire 750	GK1.5	BioLegend
CD49b	PE/Cy7	DX5	BioLegend
CD45.2	Pacific Orange	30-F11	Invitrogen
CD68	PerCP/Cy5.5	FA-11	BioLegend
CD8	FITC	53-6.7	BioLegend
CD80	PerCP/eFluor 710	16-10A1	eBioscience
CD86	APC	GL-1	BioLegend
CTLA-4	PE/Dazzle 594	UC10-4B9	BioLegend
F4/80	PerCP/Cy5.5	BM8	BioLegend
FOXP3	PE	FJK-16 s	eBioscience
IFN-γ	APC	XMG1.2	BD Pharmingen
IL-4Rα	Alexa Fluor 647	mIL4R-M1	BD Pharmingen
Ly-6G	APC/Fire 750	1A8	BioLegend
MHCII	PE/Cy7	M5/114.15.2	BioLegend
MHCII	APC/Fire 750	M5/114.15.2	BioLegend
NKp46	PE	29A1.4	BioLegend
PD-1	PE	29F.1A12	BioLegend
PD-1	PerCP/Cy5.5	29F.1A12	BioLegend
PD-L1	PE	10F.9G2	BioLegend
PD-L2	PE	TY25	BioLegend
Siglec-F	PE	1RNM44N	eBioscience

APC, allophycocyanin; PE, phycoerythrin; PerCP, peridinin chlorophyll protein.

Determination of Secreted Cytokines

The quantity of cytokines present in the BALF was analyzed in the first lavage supernatants by the LEGENDplex flow-based 13-plex mouse T helper cytokine panel kit (BioLegend, Koblenz, Germany) according to the manufacturer`s protocol.

IHC Staining

The right lung of each mouse was inflated with 0.5 mL of PBS containing 4% paraformaldehyde and fixed for 1 h at room temperature (RT), dehydrated in ascending isopropanol dilutions, and embedded in paraffin. Sections of 4 μm of three different lung layers approximately 500 μm apart from each other were analyzed for each mouse lung.

Lung specimens were rehydrated, and heat-mediated antigen retrieval was performed (10 mM citric acid buffer [pH 6.0], 20 min). Afterward, paraffin sections were blocked with 10% FBS containing 0.1% Triton X-100 for 30 min. Then, sections were stained with primary antibodies

specific to NP protein of PR8 virus (goat anti-influenza NP [G105]; kind gift of Dr. Robert Webster, Department of Infectious Diseases, St. Jude Children's Research Hospital, Memphis, TN, USA) or MC1R (Thermo Fisher Scientific, Schwerte, Germany) for 1 h at RT followed by species-specific secondary antibody incubation for 30 min. Proteins of interest were visualized by the Vectastain ABC-AP kit (Vector Laboratories, Burlingame, CA, USA) according to the producer's recommendations. For the quantitative analysis of tumor tissue, merged images of MC1R-stained sections were made using a Biorevo BZ-9000 microscope (Keyence, Neu-Isenburg, Germany), and tumor area was quantified in relationship to the whole lung section area using AxioVision software (Carl Zeiss, Oberkochen, Germany). Data for each mouse are presented as mean values of three different sections that were approximately 500 μm apart from each other.

Statistical Analysis

Data are expressed as mean ± SEM. Statistical analysis was performed using GraphPad Prism software (version 7), and the following two-tailed tests were performed as indicated in the figure legends: Mann-Whitney U test; Kruskal-Wallis test followed by Dunn's comparison analysis; one-way ANOVA followed by Dunnett's multiple comparison test; or two-way ANOVA, followed by Sidak's multiple comparisons test. Results were considered statistically significant at $p < 0.05$ and are displayed as $*p < 0.05$, $**p < 0.01$, $***p < 0.001$, and $****p < 0.0001$.

SUPPLEMENTAL INFORMATION

Supplemental Information can be found online at https://doi.org/10.1016/j.omto.2020.03.023.

AUTHOR CONTRIBUTIONS

S.S., D.M., and V.W. conceived and designed the experiments. S.S., D.M., and R.L.D. performed the experiments and statistical data analysis. All authors participated in the discussion and interpretation of data. V.W. and S.L. supervised all experimental work. S.S., D.M., and V.W. wrote the paper. All authors read and approved the final manuscript.

CONFLICTS OF INTEREST

The authors declare no competing interests.

ACKNOWLEDGMENTS

REFERENCES

1. Pastorino, U. (2010). The development of an international registry. J. Thorac. Oncol. 5 (6, Suppl 2), S196–S197.

2. Marzagalli, M., Ebelt, N.D., and Manuel, E.R. (2019). Unraveling the crosstalk between melanoma and immune cells in the tumor microenvironment. Semin. Cancer Biol. 59, 236–250.

3. Villanueva, J., and Herlyn, M. (2008). Melanoma and the tumor microenvironment. Curr. Oncol. Rep. 10, 439–446.

4. Masemann, D., Boergeling, Y., and Ludwig, S. (2017). Employing RNA viruses to fight cancer: novel insights into oncolytic virotherapy. Biol. Chem. 398, 891–909.

5. Martinez-Quintanilla, J., Seah, I., Chua, M., and Shah, K. (2019). Oncolytic viruses: overcoming translational challenges. J. Clin. Invest. 130, 1407–1418.

6. Masemann, D., Köther, K., Kuhlencord, M., Varga, G., Roth, J., Lichty, B.D., Rapp, U.R., Wixler, V., and Ludwig, S. (2018). Oncolytic influenza virus infection restores immunocompetence of lung tumor-associated alveolar macrophages. OncoImmunology 7, e1423171.

7. Byrne, E.H., and Fisher, D.E. (2017). Immune and molecular correlates in melanoma treated with immune checkpoint blockade. Cancer 123 (S11), 2143–2153.

8. Ludwig, S., Hrincius, E.R., and Boergeling, Y. (2019). The two sides of the same coin-influenza virus and intracellular signal transduction. Cold Spring Harb. Perspect. Med. a038513.

9. Ludwig, S., Planz, O., Pleschka, S., and Wolff, T. (2003). Influenza-virus-induced signaling cascades: targets for antiviral therapy? Trends Mol. Med. 9, 46–52.

10. Pleschka, S., Wolff, T., Ehrhardt, C., Hobom, G., Planz, O., Rapp, U.R., and Ludwig, S. (2001). Influenza virus propagation is impaired by inhibition of the Raf/MEK/ERK signalling cascade. Nat. Cell Biol. 3, 301–305.

11. Hamilton, J.R., Vijayakumar, G., and Palese, P. (2018). A recombinant antibody-expressing influenza virus delays tumor growth in a mouse model. Cell Rep. 22, 1–7.

12. van Rikxoort, M., Michaelis, M., Wolschek, M., Muster, T., Egorov, A., Seipelt, J., Doerr, H.W., and Cinatl, J., Jr. (2012). Oncolytic effects of a novel influenza A virus expressing interleukin-15 from the NS reading frame. PLoS ONE 7, e36506.

13. Pavlick, A.C., Fecher, L., Ascierto, P.A., and Sullivan, R.J. (2019). Frontline therapy for BRAF-mutated metastatic melanoma: how do you choose, and is there one correct answer? Am. Soc. Clin. Oncol. Educ. Book 39, 564–571.

14. Robert, C., Schachter, J., Long, G.V., Arance, A., Grob, J.J., Mortier, L., Daud, A., Carlino, M.S., McNeil, C., Lotem, M., et al.; KEYNOTE-006 Investigators (2015). Pembrolizumab versus ipilimumab in advanced melanoma. N. Engl. J. Med. 372, 2521–2532.

15. Márquez-Rodas, I., Cerezuela, P., Soria, A., Berrocal, A., Riso, A., González-Cao, M., and Martín-Algarra, S. (2015). Immune checkpoint inhibitors: therapeutic advances in melanoma. Ann. Transl. Med. 3, 267.

16. Rajani, K., Parrish, C., Kottke, T., Thompson, J., Zaidi, S., Ilett, L., Shim, K.G., Diaz, R.M., Pandha, H., Harrington, K., et al. (2016). Combination therapy with reovirus and anti-PD-1 blockade controls tumor growth through innate and adaptive immune responses. Mol. Ther. 24, 166–174.

17. Zamarin, D., Ricca, J.M., Sadekova, S., Oseledchyk, A., Yu, Y., Blumenschein, W.M., Wong, J., Gigoux, M., Merghoub, T., and Wolchok, J.D. (2018). PD-L1 in tumor microenvironment mediates resistance to oncolytic immunotherapy. J. Clin. Invest. 128, 1413–1428.

18. Fidler, I.J. (1973). Selection of successive tumour lines for metastasis. Nat. New Biol. 242, 148–149.

19. Köther, K., Nordhoff, C., Masemann, D., Varga, G., Bream, J.H., Gaestel, M., Wixler, V., and Ludwig, S. (2014). MAPKAP kinase 3 suppresses Ifng gene expression and attenuates NK cell cytotoxicity and Th1 CD4 T-cell development upon influenza A virus infection. FASEB J. 28, 4235–4246.

20. Masemann, D., Leite Dantas, R., Sitnik, S., Schied, T., Nordhoff, C., Ludwig, S., and Wixler, V. (2018). The four-and-a-half LIM domain protein 2 supports influenza a virus-induced lung inflammation by restricting the host adaptive immune response. Am. J. Pathol. 188, 1236–1245.

21. Ghoneim, H.E., Thomas, P.G., and McCullers, J.A. (2013). Depletion of alveolar macrophages during influenza infection facilitates bacterial superinfections. J. Immunol. 191, 1250–1259.

22. Shirey, K.A., Pletneva, L.M., Puche, A.C., Keegan, A.D., Prince, G.A., Blanco, J.C., and Vogel, S.N. (2010). Control of RSV-induced lung injury by alternatively activated macrophages is IL-4Rα-, TLR4-, and IFN-β-dependent. Mucosal Immunol. 3, 291–300.

23. Ayukawa, H., Matsubara, T., Kaneko, M., Hasegawa, M., Ichiyama, T., and Furukawa, S. (2004). Expression of CTLA-4 (CD152) in peripheral blood T cells of children with

influenza virus infection including encephalopathy in comparison with respiratory syncytial virus infection. Clin. Exp. Immunol. *137*, 151–155.

24. McNally, B., Ye, F., Willette, M., and Flaño, E. (2013). Local blockade of epithelial PDL-1 in the airways enhances T cell function and viral clearance during influenza virus infection. J. Virol. *87*, 12916–12924.

25. Rojas, J.J., Sampath, P., Hou, W., and Thorne, S.H. (2015). Defining effective combinations of immune checkpoint blockade and oncolytic virotherapy. Clin. Cancer Res. *21*, 5543–5551.

26. Flaherty, K.T., Infante, J.R., Daud, A., Gonzalez, R., Kefford, R.F., Sosman, J., Hamid, O., Schuchter, L., Cebon, J., Ibrahim, N., et al. (2012). Combined BRAF and MEK inhibition in melanoma with BRAF V600 mutations. N. Engl. J. Med. *367*, 1694–1703.

27. Lito, P., Rosen, N., and Solit, D.B. (2013). Tumor adaptation and resistance to RAF inhibitors. Nat. Med. *19*, 1401–1409.

28. Bommareddy, P.K., Patel, A., Hossain, S., and Kaufman, H.L. (2017). Talimogene laherparepvec (T-VEC) and other oncolytic viruses for the treatment of melanoma. Am. J. Clin. Dermatol. *18*, 1–15.

29. Johnson, D.B., Puzanov, I., and Kelley, M.C. (2015). Talimogene laherparepvec (T-VEC) for the treatment of advanced melanoma. Immunotherapy *7*, 611–619.

30. Overwijk, W.W., and Restifo, N.P. (2001). B16 as a mouse model for human melanoma. Curr. Protoc. Immunol. Chapter 20. Unit 20.1.

31. GeurtsvanKessel, C.H., Willart, M.A., van Rijt, L.S., Muskens, F., Kool, M., Baas, C., Thielemans, K., Bennett, C., Clausen, B.E., Hoogsteden, H.C., et al. (2008). Clearance of influenza virus from the lung depends on migratory langerin$^+$CD11b$^-$ but not plasmacytoid dendritic cells. J. Exp. Med. *205*, 1621–1634.

32. Hrincius, E.R., Hennecke, A.K., Gensler, L., Nordhoff, C., Anhlan, D., Vogel, P., McCullers, J.A., Ludwig, S., and Ehrhardt, C. (2012). A single point mutation (Y89F) within the non-structural protein 1 of influenza A viruses limits epithelial cell tropism and virulence in mice. Am. J. Pathol. *180*, 2361–2374.

33. Mazur, I., Anhlan, D., Mitzner, D., Wixler, L., Schubert, U., and Ludwig, S. (2008). The proapoptotic influenza A virus protein PB1-F2 regulates viral polymerase activity by interaction with the PB1 protein. Cell. Microbiol. *10*, 1140–1152.

34. Seyer, R., Hrincius, E.R., Ritzel, D., Abt, M., Mellmann, A., Marjuki, H., Kühn, J., Wolff, T., Ludwig, S., and Ehrhardt, C. (2012). Synergistic adaptive mutations in the hemagglutinin and polymerase acidic protein lead to increased virulence of pandemic 2009 H1N1 influenza A virus in mice. J. Infect. Dis. *205*, 262–271.

35. Börgeling, Y., Schmolke, M., Viemann, D., Nordhoff, C., Roth, J., and Ludwig, S. (2014). Inhibition of p38 mitogen-activated protein kinase impairs influenza virus-induced primary and secondary host gene responses and protects mice from lethal H5N1 infection. J. Biol. Chem. *289*, 13–27.

36. Leite Dantas, R., Brachvogel, B., Schied, T., Bergmeier, V., Skryabin, B., Vogl, T., Ludwig, S., and Wixler, V. (2017). The LIM-only protein four and a half LIM Domain protein 2 attenuates development of psoriatic arthritis by blocking Adam17-mediated tumor necrosis factor release. Am. J. Pathol. *187*, 2388–2398.